

Metal-Organic Layers as Multifunctional 2D Nanomaterials for Enhanced Photoredox Catalysis

Guangxu Lan, Yangjian Quan, Maolin Wang, Geoffrey T Nash, Eric You, Yang Song, Samuel S. Veroneau, Xiaomin Jiang, and Wenbin Lin

J. Am. Chem. Soc., **Just Accepted Manuscript** • DOI: 10.1021/jacs.9b08956 • Publication Date (Web): 24 Sep 2019

Downloaded from pubs.acs.org on September 25, 2019

Just Accepted

“Just Accepted” manuscripts have been peer-reviewed and accepted for publication. They are posted online prior to technical editing, formatting for publication and author proofing. The American Chemical Society provides “Just Accepted” as a service to the research community to expedite the dissemination of scientific material as soon as possible after acceptance. “Just Accepted” manuscripts appear in full in PDF format accompanied by an HTML abstract. “Just Accepted” manuscripts have been fully peer reviewed, but should not be considered the official version of record. They are citable by the Digital Object Identifier (DOI®). “Just Accepted” is an optional service offered to authors. Therefore, the “Just Accepted” Web site may not include all articles that will be published in the journal. After a manuscript is technically edited and formatted, it will be removed from the “Just Accepted” Web site and published as an ASAP article. Note that technical editing may introduce minor changes to the manuscript text and/or graphics which could affect content, and all legal disclaimers and ethical guidelines that apply to the journal pertain. ACS cannot be held responsible for errors or consequences arising from the use of information contained in these “Just Accepted” manuscripts.

Metal-Organic Layers as Multifunctional 2D Nanomaterials for Enhanced Photoredox Catalysis

Guangxu Lan,^{‡,1} Yangjian Quan,^{‡,1} Maolin Wang,^{1,2} Geoffrey T. Nash,¹ Eric You,¹ Yang Song,¹ Samuel S. Veroneau,¹ Xiaomin Jiang,¹ and Wenbin Lin^{*,1}

¹Department of Chemistry, The University of Chicago, Chicago, IL 60637, USA.

²College of Chemistry and Molecular Engineering, Peking University, Beijing 100871, China.

Supporting Information Placeholder

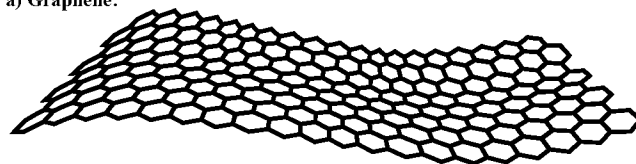
ABSTRACT: Metal-organic layers (MOLs) have recently emerged as a novel class of molecular 2D materials with significant potential for catalytic applications. Herein we report the design of a new multifunctional MOL, Hf₁₂-Ir-Ni, by laterally linking Hf₁₂ secondary building units (SBUs) with photosensitizing Ir(DBB)[dF(CF₃)ppy]₂⁺ [DBB-Ir-F, DBB = 4,4'-di(4-benzoato)-2,2'-bipyridine; dF(CF₃)ppy = 2-(2,4-difluorophenyl)-5-(trifluoromethyl)pyridine] bridging ligands and vertically terminating the SBUs with catalytic Ni(MBA)Cl₂ [MBA = 2-(4'-methyl-[2,2'-bipyridin]-4-yl)acetate] capping agents. Hf₁₂-Ir-Ni was synthesized in a bottom-up approach and characterized by TEM, AFM, PXRD, TGA, NMR, ICP-MS, UV-Vis, and luminescence spectroscopy. The proximity between photosensitizing Ir centers and catalytic Ni centers (~0.85 nm) in Hf₁₂-Ir-Ni facilitates single electron transfer, leading to a 15-fold increase in photoredox reactivity. Hf₁₂-Ir-Ni was highly effective in catalytic C-S, C-O, and C-C cross-coupling reactions with broad substrate scopes and turnover numbers of ~4500, ~1900, and ~450, respectively.

Two-dimensional (2D) materials, exemplified by graphene and transition metal dichalcogenides (TMDCs), have been intensively studied owing to their favorable electronic and optical properties.¹⁻⁴ Intrinsically high surface areas of 2D materials should in principle allow the incorporation of multiple functionalities via surface modification to mediate photocatalytic reactions.⁵⁻⁶ To date, however, the performance of 2D materials in photocatalysis has been underwhelming, often limited by poor light-harvesting efficiency or/and low catalytic activity due to the difficulty of installing disparate functionalities in a spatially controlled manner.⁷⁻⁸ It is thus of great importance to develop molecular 2D materials with synthetic flexibility and molecular tunability, allowing for hierarchical installation of multiple functionalities to afford much enhanced photocatalytic activities over their homogeneous counterparts.⁹⁻¹¹

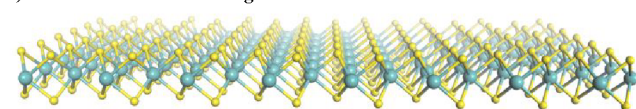
As a dispersible monolayered version of metal-organic frameworks (MOFs),¹²⁻²⁶ metal-organic layers (MOLs) have recently emerged as a novel class of molecular 2D materials with tremendous potential for catalytic applications.²⁷⁻²⁹ MOLs not only retain the advantages offered by MOFs such as structural regularity/tunability and compositional diversity but also possess the aforementioned strengths of 2D materials. Importantly, unlike graphene and TMDCs, disparate functionalities can be installed

onto the surfaces of MOLs in a spatially controlled fashion by modifying distinct functional groups on their secondary building units (SBUs) and bridging ligands to accomplish synergistic complex functions (Figure 1). Herein we report the design of a new multifunctional MOL, Hf₁₂-Ir-Ni, for highly efficient photoredox catalysis by taking advantage of the proximity between photosensitizing bridging ligands and Ni catalysts on the SBUs.

a) Graphene:



b) Transition metal dichalcogenides:



c) Metal-organic layers:

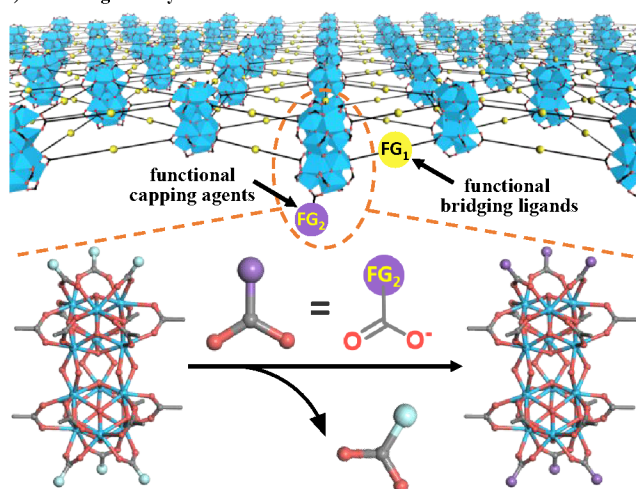


Figure 1. Schematic depiction of graphene (a), TMDCs (b), and MOLs (c). Unlike graphene and TMDCs, MOLs allow hierarchical incorporation of disparate functional groups (FGs) into both bridging linkers and capping agents. Zoomed-in view of postsynthetic surface modification of MOLs with functional capping agents through carboxylate exchange.

Hf₁₂-Ir-Ni is a 2D network built from Hf₁₂ SBUs and photosensitizing Ir(DBB)[dF(CF₃)ppy]₂⁺ [DBB-Ir-F, DBB = 4,4'-di(4-benzoato)-2,2'-bipyridine; dF(CF₃)ppy = 2-(2,4-difluorophenyl)-5-(trifluoromethyl)pyridine] bridging ligands (Figures S1-S4, SI). The SBUs are vertically terminated by catalytically active Ni(MBA)Cl₂ [MBA-Ni, MBA = 2-(4'-methyl-[2,2'-bipyridin]-4-yl)acetate] capping agents (Figures S5-S9, SI) to afford a monolayer structure. Hf₁₂-Ir-Ni was synthesized in three steps (Figures 2a and S10, SI). First, free-standing Hf₁₂-Ir-F was prepared through a solvothermal reaction between HfCl₄ and H₂DBB-Ir-F in N,N-dimethylformamide (DMF) at 80 °C with trifluoroacetic acid and water as modulators. Hf₁₂ SBUs were vertically terminated by trifluoroacetate (TFA) capping agents and

laterally bridged by DBB-Ir-F ligands to afford an infinite 2D network of the formula Hf₁₂(μ₃-O)₈(μ₃-OH)₈(μ₂-OH)₆(DBB-Ir-F)₆(TFA)₆. Second, MBA capping agents were installed on the surface of Hf₁₂-Ir-F by replacing TFA groups to afford Hf₁₂-Ir-MBA with the formula of Hf₁₂(μ₃-O)₈(μ₃-OH)₈(μ₂-OH)₆(DBB-Ir-F)₆(MBA)₆. Finally, Hf₁₂-Ir-Ni was obtained by metalating the MBA capping agents on Hf₁₂-Ir-MBA to generate catalytically active MBA-Ni. Hf₁₂-Ir-Ni has a formula of Hf₁₂(μ₃-O)₈(μ₃-OH)₈(μ₂-OH)₆(DBB-Ir-F)₆(MBA-Ni)₆ with the Ir and Ni centers in close proximity of ~0.85 nm from each other, which affords a >10-fold increase in single electron transfer (SET) and a 15-fold increase in photoredox reactivity over the homogenous control (Figure 3a).

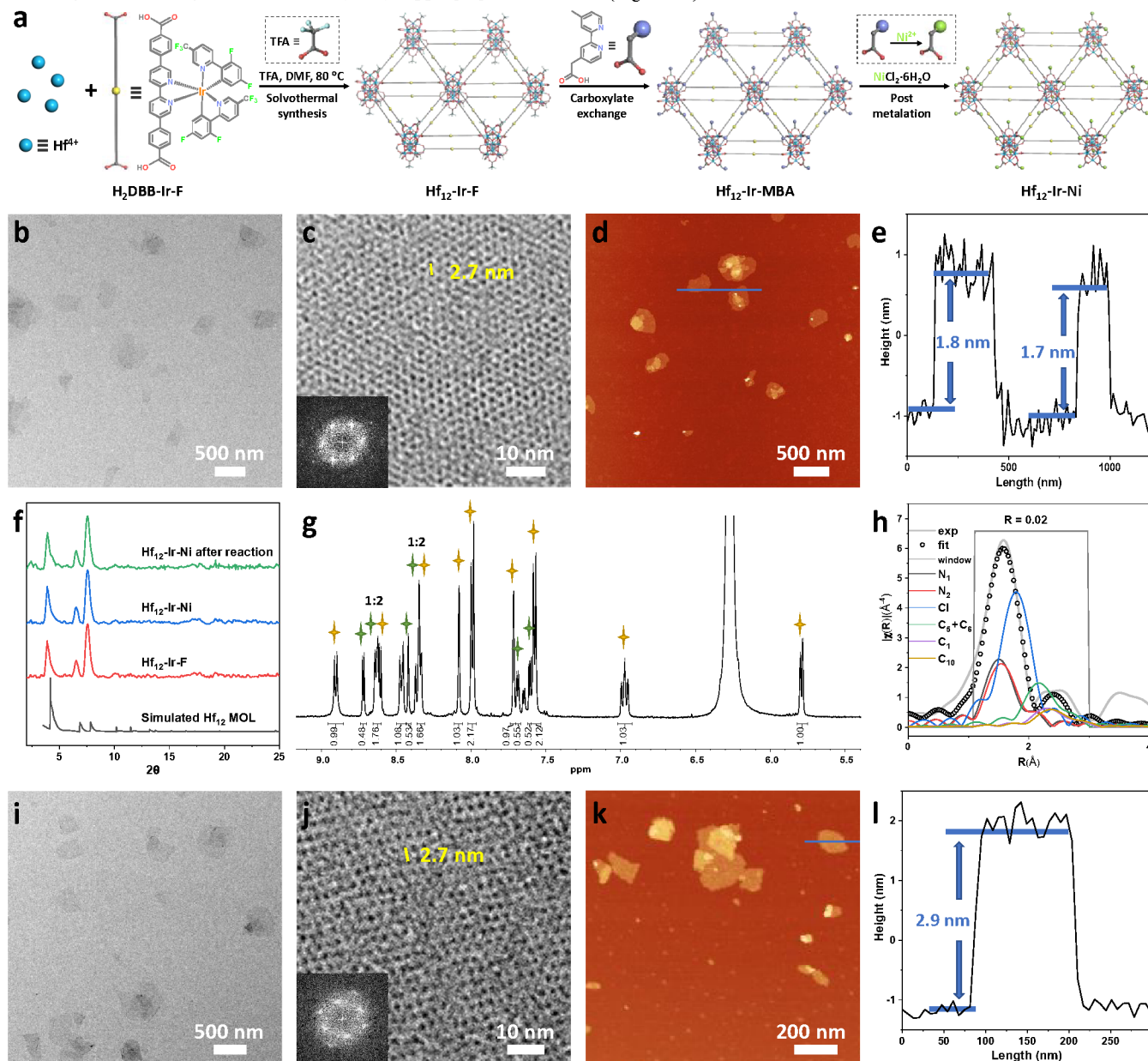


Figure 2. Synthesis and Characterization of Hf₁₂-Ir-F, Hf₁₂-Ir-MBA, and Hf₁₂-Ir-Ni. (a) Schematic showing the synthesis of Hf₁₂-Ir-Ni. (b-e) TEM image (b), HRTEM image with the FFT pattern in the inset (c), and AFM topography (d) and height profile (e) of Hf₁₂-Ir-F. (f) PXRD patterns of Hf₁₂-Ir-F and Hf₁₂-Ir-Ni, freshly prepared or after photoredox reaction, in comparison to the simulated pattern for the Hf₁₂ MOL. (g) NMR spectrum of digested Hf₁₂-Ir-MBA. Peaks labeled with yellow and green stars correspond to H₂DBB-Ir-F and H-MBA ligands, respectively. (h-l) EXAFS fitting (h), TEM image (i), HRTEM image with the FFT pattern in the inset (j), and AFM topography (k) and height profile (l) of Hf₁₂-Ir-Ni.

The monolayer structure of Hf₁₂-Ir-F was confirmed by a combination of transmission electron microscopy (TEM, Figures 2b and S11a, SI) and atomic force microscopy (AFM, Figures 2d,

e, and S11b, SI), with a diameter of ~300 nm and a thickness of ~1.8 nm. This thickness is consistent with the modeled height of Hf₁₂ clusters capped with TFA groups (~1.8 nm, Figure S21a, SI).

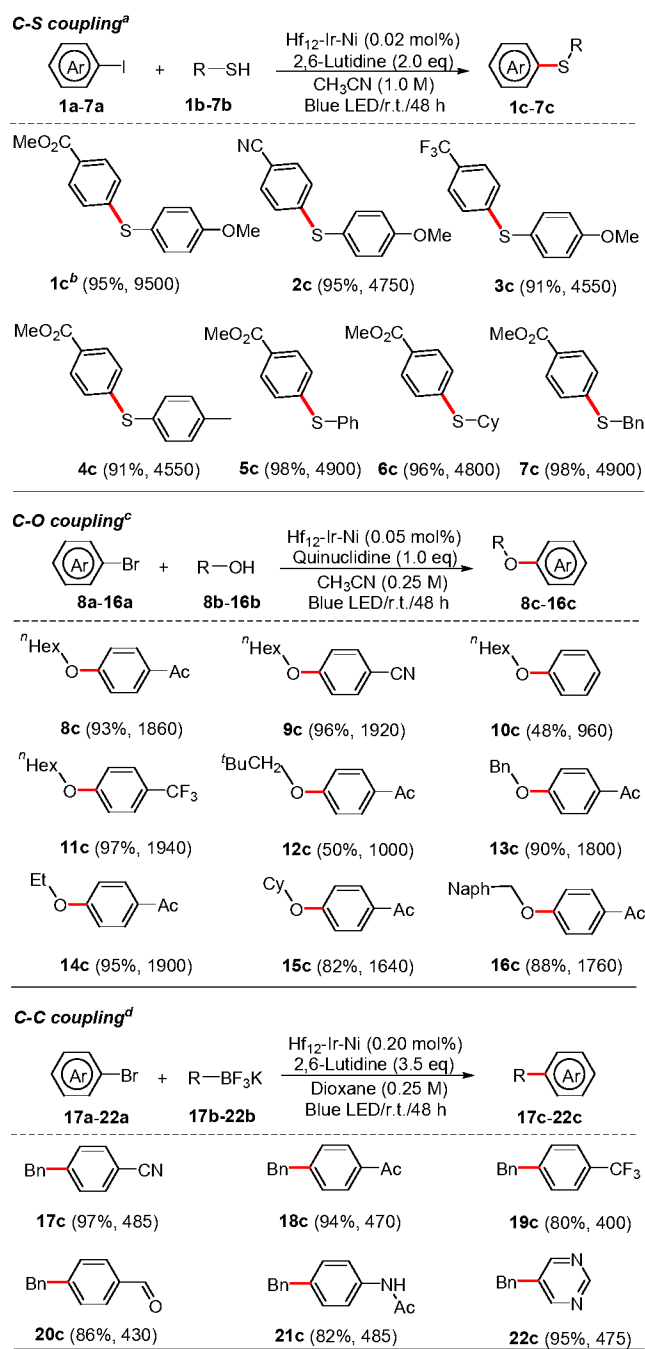
Dynamic light scattering (DLS) measurements gave a number-averaged diameter of 116.2 ± 7.3 nm for Hf₁₂-Ir-F (Figure S17, SI). The proposed **kgd** topological structure of Hf₁₂-Ir-F was supported by powder X-ray diffraction (PXRD) studies and high-resolution TEM (HRTEM) imaging. Hf₁₂-Ir-F displayed a PXRD pattern similar to that simulated based on the structure model of the Hf₁₂ MOL (Figure 2f) whereas HRTEM and its fast Fourier transform (FFT, Figure 2c) revealed a six-fold symmetry and a Hf₁₂-Hf₁₂ distance of 2.7 nm, matching well with the modeled structure (Figure S21a, SI). In addition, the ¹H NMR spectrum of digested Hf₁₂-Ir-F showed only signals corresponding to DBB-Ir-F (Figure S12, SI). Thermogravimetric analysis (TGA) of Hf₁₂-Ir-F showed a weight loss of 62.4% in the 350-800 °C range, corresponding to its decomposition to (12 HfO₂ + 6 IrO₂) (61.5% expected; Figure S13, SI). Finally, UV-Vis (Figure S18, SI) and luminescence (Figure S14, SI) spectra showed that Hf₁₂-Ir-F displayed the same characteristic absorption, excitation, and emission spectra as Me₂DBB-Ir, suggesting the photosensitizing ability of Hf₁₂-Ir-F.

Hf₁₂-Ir-F was further functionalized through exchanging weakly coordinating TFA groups on the SBUs with MBA capping agents to afford Hf₁₂-Ir-MBA. The ¹H NMR spectrum of digested Hf₁₂-Ir-MBA showed an MBA to DBB-Ir-F molar ratio of ~1:1 (Figure 2g), indicating complete replacement of TFA groups. After metalation of the MBA sites on Hf₁₂-Ir-MBA with NiCl₂, we used X-ray absorption spectroscopy to characterize the coordination environment of the MBA-Ni species. Hf₁₂-Ir-Ni showed similar extended X-ray absorption fine structure (EXAFS) features as Me-MBA-Ni, both of which were well fitted to the molecular model of tetrahedrally coordinated Ni(bpy)Cl₂ (bpy = 2,2'-bipyridine; Figures 1h, S19-20, and Table S1, SI). Inductively coupled plasma-mass spectrometry (ICP-MS) analysis indicated that Hf₁₂-Ir-Ni had a Ni to Hf molar ratio of ~1:2, matching the ratio expected for complete metalation of Hf₁₂-Ir-MBA by NiCl₂. The UV-Vis absorption spectrum of Hf₁₂-Ir-Ni displayed characteristic absorption peaks attributable to both Me₂DBB-Ir-F and Me-MBA-Ni (Figure S18, SI). TEM and AFM imaging indicated that Hf₁₂-Ir-Ni retained the monolayer structure and morphology of Hf₁₂-Ir-F, with a diameter of ~300 nm (Figures 2i and S16a, SI) and a thickness of ~2.9 nm (Figures 2k, l, and S16b, SI). The increased thickness was consistent with the modeled height of the Hf₁₂ cluster capped with MBA-Ni ligands (Figure S21b, SI). DLS measurements also showed that Hf₁₂-Ir-Ni exhibited a slightly increased size with a number-averaged diameter of 122.0 ± 2.3 nm (Figure S17, SI). Finally, Hf₁₂-Ir-Ni exhibited similar PXRD patterns (Figure 2f) and HRTEM images (Figure 2j) to Hf₁₂-Ir-F, indicating the retention of the **kgd** topological structure during postsynthetic capping ligand exchange and Ni coordination.

On the basis of the proximity between photosensitizing DBB-Ir-F bridging ligands and catalytic MBA-Ni capping groups in Hf₁₂-Ir-Ni (~0.85 nm measured from the modeled structure, Figure S22, SI), we proposed that electron transfer (ET) from photoexcited DBB-Ir-F to MBA-NiCl₂ could be greatly enhanced to promote efficient photocatalytic reactions (Figure 3a). The spatially isolated MBA-Ni sites on the MOL surface are also expected to prevent the formation of Ni^I-Ni^{II} dimers which were recently shown to lead to diminished photoredox reactivity.³⁰ Photocatalytic performance of Hf₁₂-Ir-Ni was evaluated in three important SET reactions, including C-S cross coupling between aryl iodides and thiols, C-O cross coupling between alcohols and aryl bromides, and C-C cross-coupling between potassium benzyltrifluoroborates and aryl bromides under mild conditions (visible light, room temperature, and no strong base).³¹⁻³⁹ As

shown in Table 1, Hf₁₂-Ir-Ni efficiently catalyzed all three SET reactions to afford C-S, C-O, and C-C coupling products in high yields. With very low loadings of Hf₁₂-Ir-Ni (0.02 mol%, 0.05 mol%, and 0.20 mol% based on Ni for C-S, C-O, and C-C couplings, respectively), the reactions proceeded smoothly to afford C-S, C-O, and C-C cross-coupled products with turnover numbers (TONs) of ~4500, ~1800, and ~450, respectively. In contrast, the homogenous control containing Me₂DBB-Ir-F and Me-MBA-Ni in a 1:1 molar ratio afforded low yields of cross-coupled products (**5c**: 7%, **15c**: 5%, and **20c**: 12% for C-S, C-O, and C-C cross-couplings, respectively) at the same catalyst loadings under identical conditions (Table S2, SI). 15-500 times more homogenous Ni catalysts than Hf₁₂-Ir-Ni were required to afford comparable yields of cross-coupling products (Table S2, SI).

Table 1. Hf₁₂-Ir-Ni catalyzed C-S, C-O, and C-C cross-coupling reactions under LED irradiation at 410-480 nm.



^aReactions at 0.50 mmol scale. ^b0.01 mol% catalyst was used. ^cReactions at 0.25 mmol scale. ^dReactions at 0.125 mmol scale.

Hf₁₂-Ir-Ni catalyzed cross-coupling reactions exhibit broad substrate scopes with good compatibility with many functional groups including trifluoromethyl, cyano, carbonyl, esteryl, amidyl, naphthyl and pyrimidinyl groups. Neither acidic proton nor coordinating substituents retarded the coupling reactions. Aryl halides bearing electron-withdrawing groups afforded coupling products in higher yields, due probably to their preference to undergo oxidative addition on the Ni(0) species. No reaction was observed in the absence of either MOL catalyst or light, supporting their crucial roles in these coupling reactions. Hf₁₂-Ir-Ni was stable under photocatalytic reactions as demonstrated by the retention of PXRD pattern for the recovered Hf₁₂-Ir-Ni (Figure 1f) and the leaching of <0.3% Hf, <0.6% Ir, and <0.1% Ni as

determined by ICP-MS. We further showed that Hf₁₂-Ir-Ni could be recovered and used for at least five cycles without loss of catalytic activity (Figure 3f). We have thus developed a versatile and recyclable MOL catalyst for C-C, C-O and C-S cross-coupling reactions.³¹

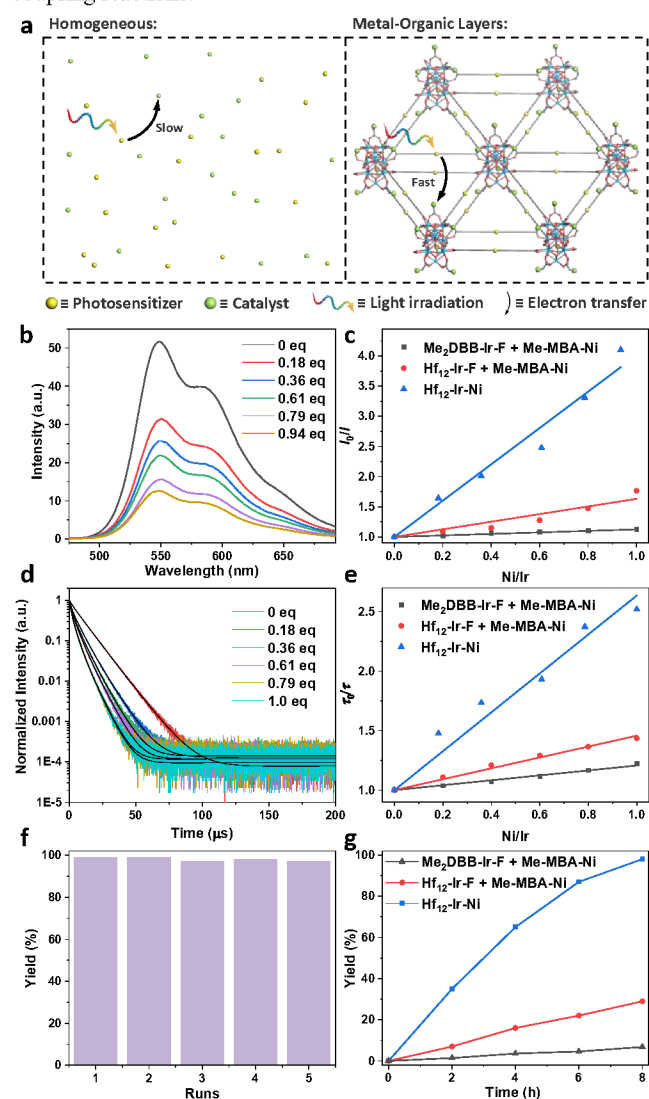


Figure 3. (a) Schematic showing enhanced SET in Hf₁₂-Ir-Ni over the homogeneous system. (b-d) Emission spectra (b) and normalized luminescence decay traces (d) of Hf₁₂-Ir-Ni with different Ni loadings. Plots of I₀/I (c) and τ₀/τ (e) as a function of the ratio of MBA-Ni to DBB-Ir-F. (f) Yields of **5c** with recovered Hf₁₂-Ir-Ni in five consecutive runs. (g) Time-dependent yields of **5c** with different catalysts.

To understand how the proximity between DBB-Ir-F and MBA-Ni in Hf₁₂-Ir-Ni impacts the photocatalytic activities, we compared ET rates from photoexcited [DBB-Ir-F]* to MBA-Ni among three different systems: a homogeneous solution of Me₂DBB-Ir-F and Me-MBA-Ni, a suspension of Hf₁₂-Ir-F and Me-MBA-Ni, and Hf₁₂-Ir-Ni. Cyclic voltammetry (CV) studies showed that [DBB-Ir-F]* could reduce MBA-Ni^{III} to MBA-Ni^I via ET (Figure S23, SI). Upon light irradiation, ET from excited [DBB-Ir-F]* to MBA-Ni led to a decrease of luminescence intensity and lifetime of [DBB-Ir-F]*, which was determined by ET rates between [DBB-Ir-F]* and MBA-Ni. These luminescence quenching curves were fitted with the following Stern-Völmer

equations with ET rates proportional to Stern-Völmer (K_{sv}) constants,

$$\frac{I_0}{I} = 1 + K_{SV}R_{Ni/Ir} \quad \text{Eq 1}$$

$$\frac{\tau_0}{\tau} = 1 + K_{SV}R_{Ni/Ir} \quad \text{Eq 2}$$

where I_0/I and τ_0/τ are the ratios of luminescence intensity and lifetime of [DBB-Ir-F]* in the absence and presence of MBA-Ni compounds, respectively, and $R_{Ni/Ir}$ represents the ratio of MBA-Ni to DBB-Ir-F in each system.

While a drastic decrease in luminescence intensity was observed in Hf₁₂-Ir-Ni with increased loading of MBA-Ni, only moderate and minimal intensity decreases were observed when Me-MBA-Ni was added to Hf₁₂-Ir-F and Me₂DBB-Ir-F, respectively (Figures 3b and S24, SI). These luminescence intensity curves were well fitted with Eq 1 to afford K_{sv} values of 3.01 ± 0.15 , 0.63 ± 0.06 , and 0.12 ± 0.01 for Hf₁₂-Ir-Ni, Hf₁₂-Ir-F, and Me₂DBB-Ir-F, respectively (Figure 3c and S24, SI). Luminescence lifetimes showed similar behaviors and were fitted to Eq 2, affording K_{sv} values of 1.64 ± 0.09 , 0.46 ± 0.01 , and 0.21 ± 0.01 for Hf₁₂-Ir-Ni, Hf₁₂-Ir-F, and Me₂DBB-Ir-F, respectively (Figures 3d, e, and S25, SI). Hf₁₂-Ir-Ni thus shows a 25-fold increase in luminescence intensity quenching and an approximately 8-fold increase in luminescence lifetime quenching over the homogenous system (Me₂DBB-Ir-F + Me-MBA-Ni), suggesting an order of magnitude enhancement in intra-MOL ET from [DBB-Ir-F]* to MBA-Ni in Hf₁₂-Ir-Ni. Hf₁₂-Ir-F shows slightly enhanced ET from [DBB-Ir-F]* to Me₂MBA-Ni, likely due to attractive interactions between Hf₁₂-Ir-F and Me-MBA-Ni. To probe how enhanced ET affects the rates of photocatalytic reactions, we studied time-dependent yields of **5c** with the three catalytic systems: Hf₁₂-Ir-Ni and Hf₁₂-Ir-F + Me-MBA-Ni showed ~15-fold and ~4-fold increases in reaction rates over the homogenous control (Me₂DBB-Ir-F + Me-MBA-Ni), respectively.

In summary, we developed a bottom-up approach to a new multifunctional MOL for efficient photoredox catalysis. Hierarchical installation of photosensitizing DBB-Ir-F bridging ligands and catalytically active MBA-Ni capping agents in close proximity (~0.85 nm) on the Hf₁₂-Ir-Ni MOL significantly enhances electron transfer from [DBB-Ir-F]* to MBA-Ni^{II}, leading to a 15-fold increase in photoredox reactivity. Hf₁₂-Ir-Ni is highly effective in catalyzing important C-S, C-O, and C-C cross-coupling reactions with broad substrate scopes and turnover numbers of ~4500, ~1900, and ~450, respectively. This work provides a general strategy for designing multifunctional MOLs for photocatalytic applications.

ASSOCIATED CONTENT

Supporting Information

The Supporting Information is available free of charge on the ACS Publications website.

Synthesis and characterization of Hf₁₂-Ir-F and Hf₁₂-Ir-Ni, photoredox reactions, and mechanism study (PDF)

AUTHOR INFORMATION

Corresponding Author

wenbinlin@uchicago.edu

Author Contributions

‡These authors contributed equally.

Notes

The authors declare no competing financial interests.

ACKNOWLEDGMENT

We thank Dr. Justin Jureller and Zhe Li for experimental help. We acknowledge the National Science Foundation for founding support and the MRSEC Shared User Facilities at the University of Chicago (NSF DMR-1420709) for instrument access. XAS analysis was performed at Beamline 10-BM, supported by the Materials Research Collaborative Access Team (MRCAT). Use of the Advanced Photon Source, an Office of Science User Facility operated for the U.S. DOE Office of Science by ANL, was supported by the U.S. DOE under Contract No. DE-AC02-06CH11357.

REFERENCES

- Manzeli, S.; Ovchinnikov, D.; Pasquier, D.; Yazyev, O. V.; Kis, A., 2D transition metal dichalcogenides. *Nature Reviews Materials* **2017**, *2*, 17033.
- Expanding our 2D vision. *Nature Reviews Materials* **2016**, *1*, 16089.
- Yang, Y.; Yang, X.; Liang, L.; Gao, Y.; Cheng, H.; Li, X.; Zou, M.; Ma, R.; Yuan, Q.; Duan, X., Large-area graphene-nanomesh/carbon-nanotube hybrid membranes for ionic and molecular nanofiltration. *Science* **2019**, *364* (6445), 1057.
- Tan, C.; Cao, X.; Wu, X.-J.; He, Q.; Yang, J.; Zhang, X.; Chen, J.; Zhao, W.; Han, S.; Nam, G.-H.; Sindoro, M.; Zhang, H., Recent Advances in Ultrathin Two-Dimensional Nanomaterials. *Chem. Rev.* **2017**, *117* (9), 6225-6331.
- Luo, B.; Liu, G.; Wang, L., Recent advances in 2D materials for photocatalysis. *Nanoscale* **2016**, *8* (13), 6904-6920.
- Low, J.; Cao, S.; Yu, J.; Wageh, S., Two-dimensional layered composite photocatalysts. *Chem. Commun.* **2014**, *50* (74), 10768-10777.
- Hasani, A.; Tekalgne, M.; Le, Q. V.; Jang, H. W.; Kim, S. Y., Two-dimensional materials as catalysts for solar fuels: hydrogen evolution reaction and CO₂ reduction. *Journal of Materials Chemistry A* **2019**, *7* (2), 430-454.
- Butler, S. Z.; Hollen, S. M.; Cao, L.; Cui, Y.; Gupta, J. A.; Gutiérrez, H. R.; Heinz, T. F.; Hong, S. S.; Huang, J.; Ismach, A. F.; Johnston-Halperin, E.; Kuno, M.; Plashnitsa, V. V.; Robinson, R. D.; Ruoff, R. S.; Salahuddin, S.; Shan, J.; Shi, L.; Spencer, M. G.; Terrones, M.; Windl, W.; Goldberger, J. E., Progress, Challenges, and Opportunities in Two-Dimensional Materials Beyond Graphene. *ACS Nano* **2013**, *7* (4), 2898-2926.
- Berardi, S.; Drouet, S.; Francàs, L.; Gimbert-Suriñach, C.; Guttentag, M.; Richmond, C.; Stoll, T.; Llobet, A., Molecular artificial photosynthesis. *Chem. Soc. Rev.* **2014**, *43* (22), 7501-7519.
- McDaniel, N. D.; Bernhardt, S., Solar fuels: thermodynamics, candidates, tactics, and figures of merit. *Dalton Trans.* **2010**, *39* (42), 10021-10030.
- Duan, L.; Bozoglian, F.; Mandal, S.; Stewart, B.; Privalov, T.; Llobet, A.; Sun, L., A molecular ruthenium catalyst with water-oxidation activity comparable to that of photosystem II. *Nat. Chem.* **2012**, *4*, 418.
- Furukawa, H.; Cordova, K. E.; O'Keeffe, M.; Yaghi, O. M., The Chemistry and Applications of Metal-Organic Frameworks. *Science* **2013**, *341* (6149), 1230444.
- Fateeva, A.; Chater, P. A.; Ireland, C. P.; Tahir, A. A.; Khimyak, Y. Z.; Wiper, P. V.; Darwent, J. R.; Rosseinsky, M. J., A Water-Stable Porphyrin-Based Metal-Organic Framework Active for Visible-Light Photocatalysis. *Angew. Chem. Int. Ed.* **2012**, *51* (30), 7440-7444.
- Mason, J. A.; Oktawiec, J.; Taylor, M. K.; Hudson, M. R.; Rodriguez, J.; Bachman, J. E.; Gonzalez, M. I.; Cervellino, A.; Guagliardi, A.; Brown, C. M.; Llewellyn, P. L.; Masciocchi, N.; Long, J. R., Methane storage in flexible metal-organic frameworks with intrinsic thermal management. *Nature* **2015**, *527*, 357.

15. Morris, W.; Briley, W. E.; Auyeung, E.; Cabezas, M. D.; Mirkin, C. A., Nucleic Acid–Metal Organic Framework (MOF) Nanoparticle Conjugates. *J. Am. Chem. Soc.* **2014**, *136* (20), 7261–7264.
16. Cui, Y.; Yue, Y.; Qian, G.; Chen, B., Luminescent Functional Metal–Organic Frameworks. *Chem. Rev.* **2012**, *112* (2), 1126–1162.
17. Zhang, Y.; Guo, J.; Shi, L.; Zhu, Y.; Hou, K.; Zheng, Y.; Tang, Z., Tunable chiral metal organic frameworks toward visible light-driven asymmetric catalysis. *Science Advances* **2017**, *3* (8), e1701162.
18. Johnson, J. A.; Zhang, X.; Reeson, T. C.; Chen, Y.-S.; Zhang, J., Facile Control of the Charge Density and Photocatalytic Activity of an Anionic Indium Porphyrin Framework via in Situ Metalation. *J. Am. Chem. Soc.* **2014**, *136* (45), 15881–15884.
19. Jiang, Y.; Park, J.; Tan, P.; Feng, L.; Liu, X.-Q.; Sun, L.-B.; Zhou, H.-C., Maximizing Photoresponsive Efficiency by Isolating Metal–Organic Polyhedra into Confined Nanoscaled Spaces. *J. Am. Chem. Soc.* **2019**, *141* (20), 8221–8227.
20. Yu, X.; Cohen, S. M., Photocatalytic Metal–Organic Frameworks for Selective 2,2,2-Trifluoroethylation of Styrenes. *J. Am. Chem. Soc.* **2016**, *138* (38), 12320–12323.
21. Liu, Y.; Howarth, A. J.; Hupp, J. T.; Farha, O. K., Selective Photooxidation of a Mustard-Gas Simulant Catalyzed by a Porphyrinic Metal–Organic Framework. *Angew. Chem. Int. Ed.* **2015**, *54* (31), 9001–9005.
22. Xu, H.-Q.; Hu, J.; Wang, D.; Li, Z.; Zhang, Q.; Luo, Y.; Yu, S.-H.; Jiang, H.-L., Visible-Light Photoreduction of CO₂ in a Metal–Organic Framework: Boosting Electron–Hole Separation via Electron Trap States. *J. Am. Chem. Soc.* **2015**, *137* (42), 13440–13443.
23. Wang, H.; Zhu, Q.-L.; Zou, R.; Xu, Q., Metal–Organic Frameworks for Energy Applications. *Chem* **2017**, *2* (1), 52–80.
24. Chen, K.; Wu, C.-D., Transformation of Metal–Organic Frameworks into Stable Organic Frameworks with Inherited Skeletons and Catalytic Properties. *Angew. Chem. Int. Ed.* **2019**, *58* (24), 8119–8123.
25. Moreau, F.; da Silva, I.; Al Smail, N. H.; Easun, T. L.; Savage, M.; Godfrey, H. G. W.; Parker, S. F.; Manuel, P.; Yang, S.; Schröder, M., Unravelling exceptional acetylene and carbon dioxide adsorption within a tetra-amide functionalized metal-organic framework. *Nat. Commun.* **2017**, *8*, 14085.
26. Yaghi, O. M., Reticular Chemistry in All Dimensions. *ACS Central Science* **2019**, *5* (8), 1295–1300.
27. Lan, G.; Ni, K.; Xu, R.; Lu, K.; Lin, Z.; Chan, C.; Lin, W., Nanoscale Metal–Organic Layers for Deeply Penetrating X-ray-Induced Photodynamic Therapy. *Angew. Chem.* **2017**, *129* (40), 12270–12274.
28. Lan, G.; Li, Z.; Veroneau, S. S.; Zhu, Y.-Y.; Xu, Z.; Wang, C.; Lin, W., Photosensitizing Metal–Organic Layers for Efficient Sunlight-Driven Carbon Dioxide Reduction. *J. Am. Chem. Soc.* **2018**, *140* (39), 12369–12373.
29. Cao, L.; Lin, Z.; Peng, F.; Wang, W.; Huang, R.; Wang, C.; Yan, J.; Liang, J.; Zhang, Z.; Zhang, T.; Long, L.; Sun, J.; Lin, W., Self-Supporting Metal–Organic Layers as Single-Site Solid Catalysts. *Angew. Chem. Int. Ed.* **2016**, *55* (16), 4962–4966.
30. Sun, R.; Qin, Y.; Ruccolo, S.; Schnedermann, C.; Costentin, C.; Daniel, G. N., Elucidation of a Redox-Mediated Reaction Cycle for Nickel-Catalyzed Cross Coupling. *J. Am. Chem. Soc.* **2019**, *141* (1), 89–93.
31. Twilton, J.; Le, C.; Zhang, P.; Shaw, M. H.; Evans, R. W.; MacMillan, D. W. C., The merger of transition metal and photocatalysis. *Nature Reviews Chemistry* **2017**, *1*, 0052.
32. Tellis, J. C.; Primer, D. N.; Molander, G. A., Single-electron transmetalation in organoboron cross-coupling by photoredox/nickel dual catalysis. *Science* **2014**, *345* (6195), 433.
33. Terrett, J. A.; Cuthbertson, J. D.; Shurtleff, V. W.; MacMillan, D. W. C., Switching on elusive organometallic mechanisms with photoredox catalysis. *Nature* **2015**, *524*, 330.
34. Oderinde, M. S.; Frenette, M.; Robbins, D. W.; Aquila, B.; Johannes, J. W., Photoredox Mediated Nickel Catalyzed Cross-Coupling of Thiols With Aryl and Heteroaryl Iodides via Thiyl Radicals. *J. Am. Chem. Soc.* **2016**, *138* (6), 1760–1763.
35. Corcé, V.; Chamoreau, L.-M.; Derat, E.; Goddard, J.-P.; Ollivier, C.; Fensterbank, L., Silicates as Latent Alkyl Radical Precursors: Visible-Light Photocatalytic Oxidation of Hypervalent Bis-Catecholato Silicon Compounds. *Angew. Chem. Int. Ed.* **2015**, *54* (39), 11414–11418.
36. Nakajima, K.; Nojima, S.; Nishibayashi, Y., Nickel- and Photoredox-Catalyzed Cross-Coupling Reactions of Aryl Halides with 4-Alkyl-1,4-dihydropyridines as Formal Nucleophilic Alkylation Reagents. *Angew. Chem. Int. Ed.* **2016**, *55* (45), 14106–14110.
37. Welin, E. R.; Le, C.; Arias-Rotondo, D. M.; McCusker, J. K.; MacMillan, D. W. C., Photosensitized, energy transfer-mediated organometallic catalysis through electronically excited nickel(II). *Science* **2017**, *355* (6323), 380.
38. Tasker, S. Z.; Jamison, T. F., Highly Regioselective Indoline Synthesis under Nickel/Photoredox Dual Catalysis. *J. Am. Chem. Soc.* **2015**, *137* (30), 9531–9534.
39. Ackerman, L. K. G.; Martinez Alvarado, J. I.; Doyle, A. G., Direct C–C Bond Formation from Alkanes Using Ni-Photoredox Catalysis. *J. Am. Chem. Soc.* **2018**, *140* (43), 14059–14063.

TOC Graphic:

